

## Removal of $\text{Cu}^{2+}$ Ions Using Activated Carbon from Palm Kernel Shell Waste by Liquid Smoke Activation

Muhammad Faisal<sup>a,1</sup>, Abubakar<sup>a,2</sup>, Sandi Putra Kelana<sup>a,3</sup>, Dodi Eko Nanda<sup>a,4</sup>, Hiroyuki Daimon<sup>b</sup>

<sup>a</sup> Department of Chemical Engineering, Syiah Kuala University, Jl. Syech A. Rauf, Darussalam, Banda Aceh, Aceh, 23111, Indonesia  
E-mail: <sup>1</sup>mfaisal@unsyiah.ac.id; <sup>2</sup>tgk\_abakar@yahoo.com; <sup>3</sup>sandiputrakelana@gmail.com; <sup>4</sup>dodiekonanda13@gmail.com

<sup>b</sup> Department of Environmental and Life Science, Toyohashi University of Technology, Toyohashi, Aichi, Japan  
E-mail: daimon@ens.tut.ac.jp

**Abstract**— Copper ( $\text{Cu}^{2+}$ ) ions has been recognized as hazardous heavy metal and having negative effects on human health, animal, plants, and environment. Therefore, the removal of  $\text{Cu}^{2+}$  from contaminated water to an acceptable level is necessary. In this research, activated carbon prepared from palm kernel shell waste products has been used for the removal of  $\text{Cu}^{2+}$  ions from aqueous solutions. The oil palm shells were pyrolyzed at 380 °C, producing charcoal and liquid smoke. The carbon material was modified to nano size and activated by liquid smoke to generate activated carbon with a well developed porous structure and distribution porosity. The activated carbon was then characterized by Fourier-transform infrared spectroscopy (FTIR) and Scanning electron microscopy (SEM). All experiments were conducted in a batch process with initial metal concentrations in the range 30–150 ppm, contact times in the range 30–150 min and at room temperature. The best conditions for high removal efficiency of  $\text{Cu}^{2+}$  was investigated. The adsorption isotherm of the Langmuir and Freundlich models were used to analyze the data obtained. The kinetic of first and second-order models were also studied. The highest removal efficiency of 97.5% was obtained at a contact time of 60 min, an initial  $\text{Cu}^{2+}$  concentration of 30 ppm, and an agitation speed of 200 rpm. The Freundlich isotherm model was well fitted ( $R^2=0.937$ ) and indicated pseudo-first-order chemisorption. Based on the results, the activated carbon with liquid smoke activation would be an alternative adsorbent in removing  $\text{Cu}^{2+}$  from industrial wastewater.

**Keywords**— adsorption; activated carbon; nanoparticles; liquid smoke;  $\text{Cu}^{2+}$  removal.

### I. INTRODUCTION

Heavy metals are among the inorganic materials attributed to causing severe problems in the environment [1]. In the human body, a high concentration of heavy metals can be toxic, and their accumulation is associated with several health problems, including cancer, kidney failure, as well as brain and heart diseases [2], [3]. One such dangerous heavy metal is copper (Cu). Despite its importance as a micronutrient for all living things, Cu can also produce a toxic effect when its level exceeds the tolerable limit. The maximum permissible contamination level of  $\text{Cu}^{2+}$  in industrial wastewater is 1.3 mg L<sup>-1</sup> [4], [5]. Copper is widely found in wastewater from the electroplating, textile, galvanizing, fertilizer, mining, paper and pulp, and fungicide industries [6], [7].

Several methods have been proposed to remove various heavy metals from industrial wastewaters, including ionic exchange, electrochemical, membrane technologies, solid-phase extraction, precipitation, evaporation recovery, and adsorption [8]-[10]. Of these methods, the adsorption

technique is the most efficient, versatile, and economical to remove heavy metals from wastewater. Adsorption processes are also capable of producing high-quality output from liquid waste treatment, with flexible process design and operation. Adsorbents can also be reused by applying a desorption process. Various types of adsorbents such as hydroxyapatite, metal oxides, mud, zeolites, alumina, carbon nanotubes, grape bagasse, chitosan, and rice husk have been used to remove heavy metals from wastewater. The adsorption method has developed very rapidly with the advent of new nano-sized adsorbents. Nanoparticle adsorbents are increasingly being used because, in addition to offering a large contaminant removal capacity and a rapid and reactive separation process in removing contaminants, they also show a high separation efficiency for reuse [11]-[13].

Studies have been carried out to examine the adsorption of  $\text{Cu}^{2+}$  ions, as exemplified by those using N-(2-carboxyethyl) chitosan [14], bamboo and activated carbon from coconut shell [15], papaya seed activated carbon [16], active bentonite [17], chitosan-zeolite composites [18], alginate beads [19], Schwertmannite modified with

aluminium phosphate [20], and a nanocomposite based on black wattle tannin [21].

The use of such types of activated carbon to adsorb heavy metals has prompted researchers to find low-cost adsorbent materials to purify heavy metal-contaminated water. Moreover, activating agents applied to date have included hydrochloric acid, sulfuric acid, sodium hydroxide, and toluene and acetone and other chemical compounds with a potentially harmful effect on the environment. Thus, the selection of environmentally friendly activating agents is also an important issue that researchers should consider. One such adsorbent is charcoal derived from the pyrolysis residue of oil palm shell (in liquid smoke production), which has not hitherto been widely utilized [22]. The current research has aimed to investigate the efficiency and kinetics of  $\text{Cu}^{2+}$  adsorption by using nanocarbon derived from palm oil pyrolysis residue activated by liquid smoke; that is to say, exposed to compounds derived from biomass pyrolysis containing carboxylic acid, phenol, ketone, and aldehyde groups [23]. The use of residual charcoal and liquid smoke as its activating agent is expected to produce an inexpensive and effective adsorbent for  $\text{Cu}^{2+}$  adsorption.

## II. MATERIALS AND METHOD

### A. Preparation of the Adsorbent Material

Charcoal as the raw material was obtained from the residue of liquid smoke production through the pyrolysis of oil palm shells at 380 °C. Fig. 1 shows a diagram of charcoal and liquid smoke production. The procedure for which has been described in detail in a previous study [23,24].

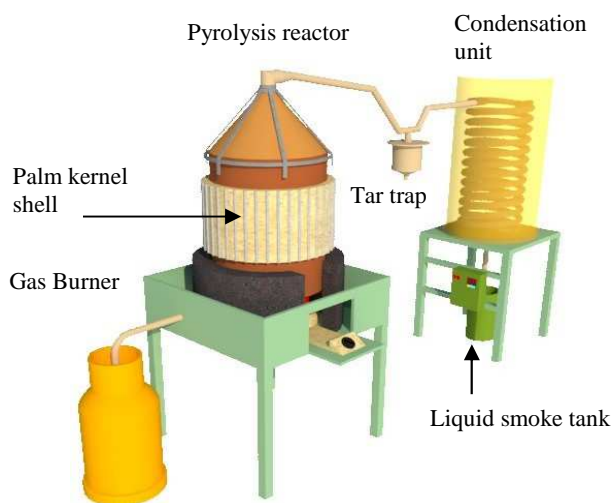


Fig. 1 Diagram of charcoal and liquid smoke production

Before use as an activator, liquid smoke was distilled at 200 °C to remove impurities. Charcoal was ball-milled (PM 100-RETSCH, Shimadzu, Japan) and made into nanoparticles. The activation process was carried out by immersing the material in liquid smoke for 24 h. The carbon nanoparticles were then collected by filtration, washed several times with aquadest, and then dried to constant weight in an oven at 105 °C to remove remaining water [23]. The schematic diagram of the adsorbent preparation can be seen in Fig.2. The structure of the charcoal before and after liquid smoke activation was examined using Fourier-

transform infrared spectroscopy (FTIR Prestige-21, Shimadzu, Japan) and Scanning electron microscopy (JEOL-JSM 6510 LA, Shimadzu, Japan). The activated carbon nanoparticles from palm shell charcoal were then stored in a desiccator before use.

### B. Adsorption Tests

The activated carbon nanoparticles were used to adsorb  $\text{Cu}^{2+}$  from  $\text{CuSO}_4$  solutions of various concentrations, specifically 30, 60, 90, 120, and 150 mg/L. Aliquots (100 mL) of  $\text{CuSO}_4$  solution were placed in a series of Erlenmeyer flasks, along with 1 g portions of activated carbon nanoparticles as the adsorbent. The mixtures were magnetically stirred at 100 and 200 rpm for contact times of 30, 60, 90, 120, and 150 min at room temperature. When the adsorption process was complete, the filtrate was centrifuged to separate any residual adsorbent. Finally, the concentration of  $\text{Cu}^{2+}$  after adsorption was tested using AAS (AA-7000, Shimadzu, Japan).

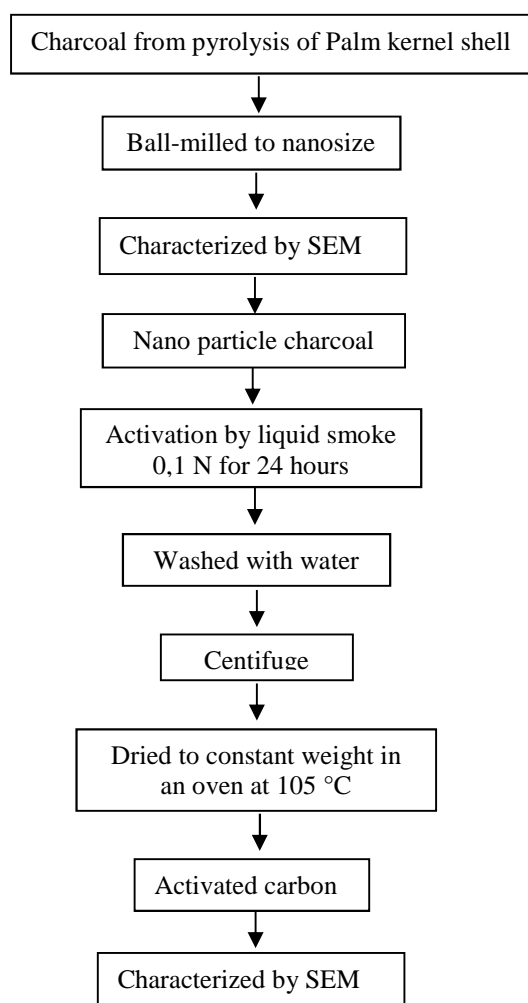


Fig. 2 Schematic diagram of adsorbent preparation

## III. RESULTS AND DISCUSSION

### A. Surface Morphology of the Adsorbent

SEM images of the palm shell charcoal from pyrolysis residue before and after chemical activation using liquid smoke are shown in Fig. 3 (a, b), respectively. As can be seen in Fig. 3 (a), the surface of the palm shell before

chemical activation had particle sizes in the range 300 nm – 1µm, with few particles as small as nanometer size. In contrast, Fig. 3 (b) shows many particles of size below 500 nm. Particles on the activated carbon were, on average,

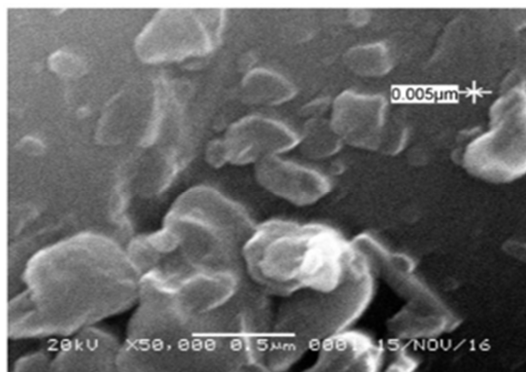
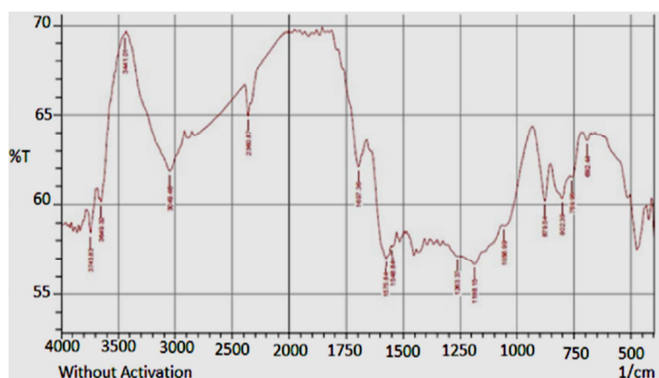


Fig. 3a SEM images of the palm shell charcoal from pyrolysis residue before activation

The corresponding FTIR spectra of palm kernel shells adsorbent before and after activation using liquid smoke can be seen in Fig.4. The amount of hydrogen and oxygen bonds was reduced after activation with liquid smoke [24], [25]. The carbon-hydrogen group was also found in the wavelength range of 3000-2700cm<sup>-1</sup> as has been reported by Ma et al. [26]



much smaller than those before chemical activation. This suggests that activation under acidic conditions can reduce the size of the activated carbon particles.

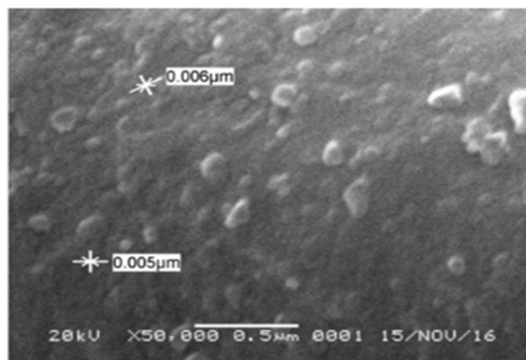


Fig. 3b SEM images of the palm shell charcoal from pyrolysis residue after the chemical activation using liquid smoke

These results agree with a study by Wu et al. [27], who found that activated carbon can easily dissolve in an acidic medium. The SEM images of the activated carbon nanoparticle adsorbent showed particle sizes in the nanometer range for both samples. The surface of the activated carbon nanoparticles was uneven, but the nanometer-sized particles were most prevalent.

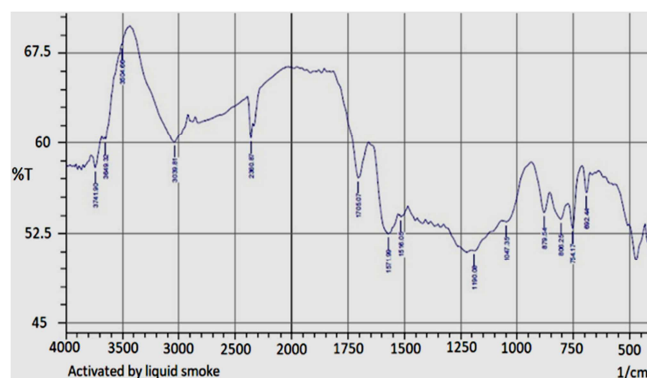


Fig. 4 FTIR spectra of adsorbent [24]

The corresponding FTIR spectra of palm kernel shells adsorbent before and after activation using liquid smoke can be seen in Fig.4. The amount of hydrogen and oxygen bonds was reduced after activation with liquid smoke [24], [25]. The carbon-hydrogen group was also found in the wavelength range of 3000-2700cm<sup>-1</sup> as has been reported by Ma et al. [26]. These results agree with a study by Wu et al. [27], who found that activated carbon can easily dissolve in an acidic medium. The SEM images of the activated carbon nanoparticle adsorbent showed particle sizes in the nanometer range for both samples. The surface of the activated carbon nanoparticles was uneven, but the nanometer-sized particles were most prevalent.

### B. Study of the Adsorption Process

1) *Effect of Contact Time on Adsorption Percentage:* The relationship between contact time and the amount of Cu<sup>2+</sup> ions adsorbed is presented in Fig. 5.

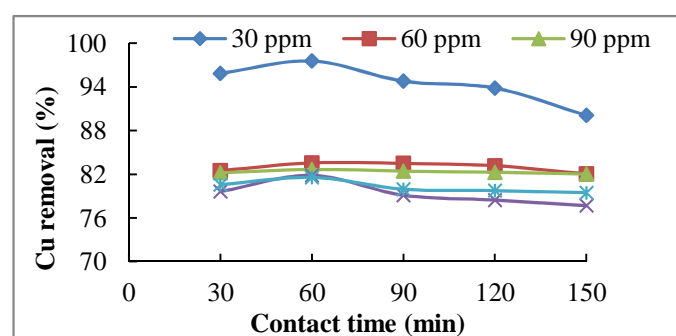


Fig. 5 The effect of contact time on Cu<sup>2+</sup> percentage removal at a various adsorbent concentration.

From Fig. 5, it is evident that between 30 and 90 min, the removal of Cu<sup>2+</sup> ions increased but then decreased with time. The optimum contact time was 60 min, after which the percentage of reduction decreased significantly. After a contact time of 150 min, the adsorbent may have been

saturated, such that its ability to retain Cu was decreased. The reduced adsorption ability of the activated nanocarbon may be attributed to Cu<sup>2+</sup> ions covering the pores on its surface. He et al. [28] found that the amount of substance held by an adsorbent tended to decrease due to the saturation of the active centers on its surface.

2) *Effect of Initial Cu<sup>2+</sup> Concentration on Adsorption Percentage:* The relationship between initial Cu<sup>2+</sup> concentration in solution and the adsorbed amount of Cu<sup>2+</sup> ions is presented in Fig. 6.

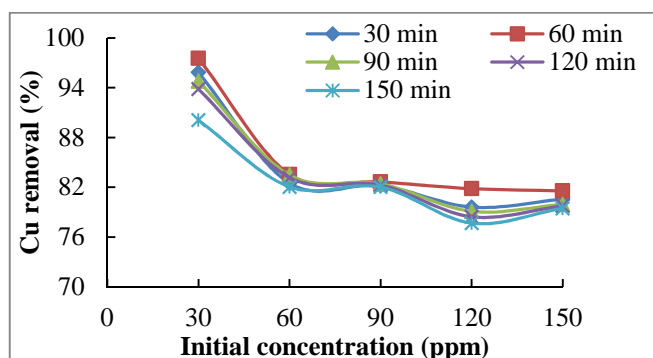


Fig. 6 Effect of initial Cu<sup>2+</sup> concentration on percentage removal of Cu<sup>2+</sup> at various contact time.

From Fig. 6, it is clear that the adsorption of Cu<sup>2+</sup> varied according to its initial concentration. The highest adsorption percentage of 97.5% was achieved at 30 ppm, whereas the lowest adsorption was seen at 120 ppm. The higher the concentration of Cu<sup>2+</sup> in the solution, the lower the adsorption percentage. This was because the dose of adsorbent used was fixed, while the adsorbate load was increased, thus leading to a lower percentage of Cu<sup>2+</sup> removal.

An increase in the initial concentration of Cu<sup>2+</sup> caused an increase in the driving force that may have affected the gradient concentration for mass transfer during the adsorption process [29,30]. At concentrations of 47.60–482.82 mg/L, the percentage of removal decreased from 94.22 to 46.93%. This is consistent with previously conducted studies [20,27], whereby the optimal concentration showing the best efficiency in the adsorption process was below 60 mg/L.

### 3) Effect of Agitation Speed on Adsorption Percentage

The interplay between contact time and the amount of Cu<sup>2+</sup> ions adsorbed at two different agitation speeds is presented in Fig. 7.

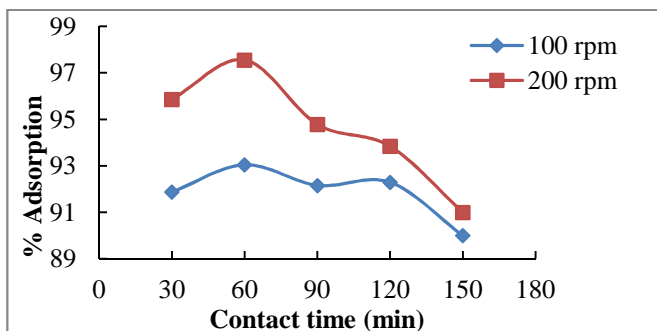


Fig. 7 The interplay between contact time and amount of adsorbed Cu<sup>2+</sup> ions at two different agitation speeds

Fig. 7 shows that at the higher agitation speed, the adsorption of Cu<sup>2+</sup> ions was greater, presumably because of more contact between Cu<sup>2+</sup> ions and the adsorbent. At 30 ppm with 30 min contact time, the adsorbent retained 95.8% of the Cu<sup>2+</sup> ions at 200 rpm, as compared to 91.8% at 100 rpm. A very low agitation speed will cause the adsorption process to run slowly. In contrast, extremely high speed will quickly damage the adsorbent structure before it has time to form a strong bond with the target metal ions. In other words, an optimum speed is required to obtain the best result. In this study, the optimum agitation speed was identified as 200 rpm, resulting in adsorption of 95.8%.

4) *Adsorption Isotherm:* The adsorption isotherm can be used to determine the interaction between a solution and an adsorbent and the optimum capacity that the adsorbent could achieve. It is a very important parameter in adsorption as it is central to determining the conditions to produce optimal adsorption. In this study, the distribution of Cu<sup>2+</sup> ions in the adsorption process between the liquid and solid phases was fitted to the mainly used models of Langmuir and Freundlich adsorption isotherm [1-4].

Langmuir equations:

$$\frac{C_e}{Q_e} = \frac{1}{q_m K_l} + \frac{C_e}{q_m} \quad (1)$$

Freundlich equations:

$$\log Q_e = \log K_f + \frac{1}{n} \log C_e \quad (2)$$

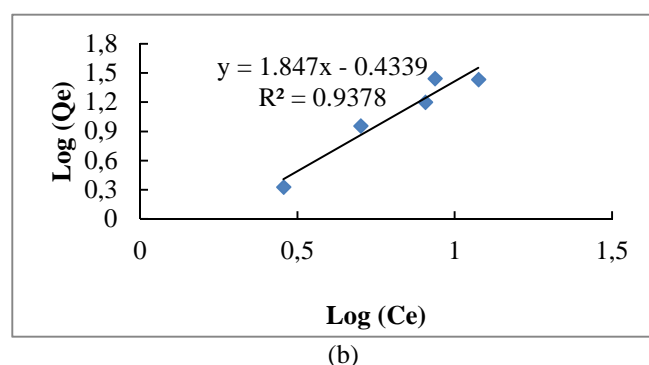
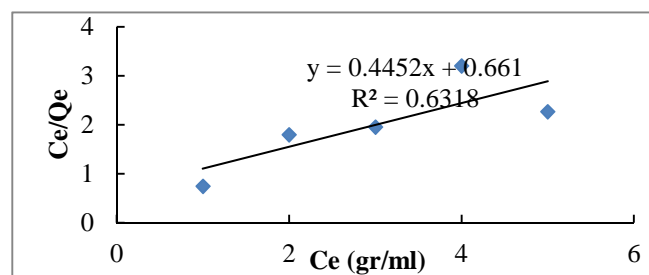


Fig. 8 (a) Langmuir and (b) Freundlich isotherm plots for the liquid-smoke-activated adsorbent

Langmuir adsorption isotherms of Cu<sup>2+</sup> ions were obtained by plotting the relationship between C<sub>e</sub> and C<sub>e</sub>/Q<sub>e</sub>. The Langmuir isotherm plot for the liquid-smoke-activated adsorbent is presented in Fig. 8 (a). The Freundlich isotherm was obtained by plotting the relationship between log C<sub>e</sub> and log q<sub>e</sub>, as shown in Fig. 8 (b).

From Fig.8 (a), it can be seen that the adsorption of  $\text{Cu}^{2+}$  by liquid-smoke-activated carbon nanoparticles could be fitted to the Freundlich isotherm model, as evidenced by a determinant coefficient ( $R^2$ ) of 0.937, whereas for the Langmuir equation model,  $R^2$  was only 0.631. This implied that the pores formed in the activated carbon nanoparticles were heterogeneous, such that the adsorbed  $\text{Cu}^{2+}$  ions could form a multilayer lining on the surface structure of the adsorbent. In adsorption, according to the Freundlich model, the amount of adsorbed substance increases relatively rapidly as the concentration is increased, and becomes slower when the adsorbate has covered the adsorbent surface. Adsorption capacity and constant value for both the Langmuir and Freundlich models of  $\text{Cu}^{2+}$  adsorption by activated carbon nanoparticles are showed in Table 1.

TABLE I  
ADSORPTION CAPACITY AND CONSTANT VALUES OF BOTH LANGMUIR AND FREUNDLICH MODELS OF  $\text{Cu}^{2+}$  METAL ADSORPTION BY ACTIVATED CARBON NANOPARTICLE

Langmuir			Freundlich		
$R^2$	$q_m$ ( $\frac{m}{g}$ )	$K_l$ ( $\frac{L}{mg}$ )	$R^2$	$n$	$K_f$ ( $\frac{mg}{g}$ )
0.631	2.24	0.673	0.937	0.541	0.368

Based on the isotherm equation used in the Langmuir model, the maximum capacity ( $q_m$ ) in the adsorption by liquid-smoke-activated carbon nanoparticles was evaluated as 2.24 L/mg, with a Langmuir constant of 0.673 mg/g. In the Freundlich isotherm model, the Freundlich empirical constant ( $K_f$ ) is 0.368 mg/g, and the Freundlich exponent ( $n$ ) is 0.541. The Freundlich exponent shows the diversity of free energy associated with the adsorption of solutes by the heterogeneous adsorbent. A value of  $1/n$  greater than 1 indicates that the adsorbate is bound with greater free energy. From the Freundlich exponent, the obtained  $n$  value here was 0.541.

5) *Adsorption Kinetics*: The adsorption kinetics of  $\text{Cu}^{2+}$  ions could be used to design the experimental system. The kinetic model used to interpret the data consisted of first- and second-order models. These models describe the adsorption mechanism, which is dependent on the adsorbent characteristics (physical and/or chemical) and the mass-transfer process. The adsorption rate constant ( $k_1$ ) for  $\text{Cu}^{2+}$  ions was evaluated according to the rate and adsorption mechanisms. The larger the value of  $k_1$ , the greater the adsorption rate. To evaluate the rate and adsorption mechanisms, first- and second-order equations were used [27]:

First-order rate equation:

$$\ln(q_e - q_t) = \ln q_e - K_1 t \quad (3)$$

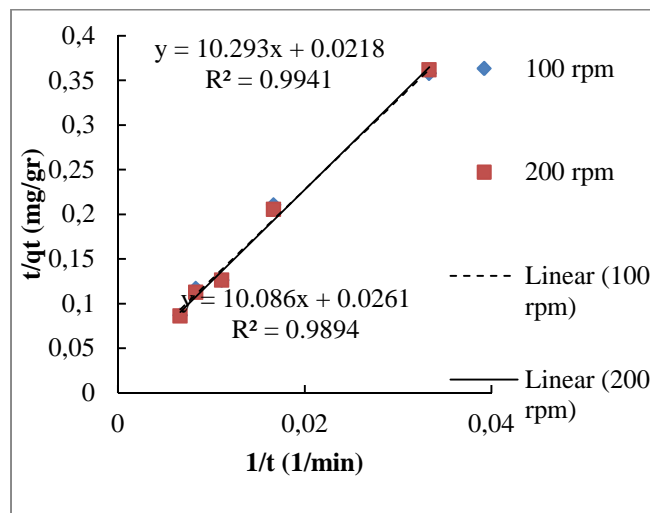
where  $q_e$  (mol/g) is the amounts adsorbed at equilibrium;  $q_t$  (mol/g) is the amounts adsorbed at the initial concentration;  $k_1$  is the first-order adsorption rate constant ( $\text{min}^{-1}$ ), and  $t$  is the adsorption time. Slope and intercept were obtained by plotting  $1/q_t$  vs  $1/t$  to obtain the reaction rate constant. The slope and intercept obtained were  $k_1/q_e$  and  $1/q_e$ .

Second-order rate equation:

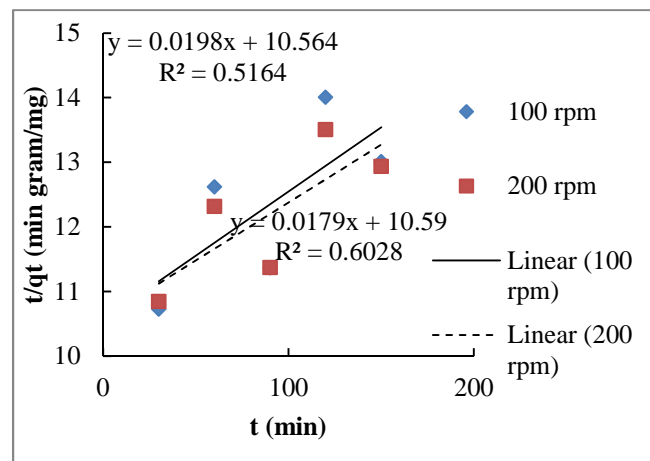
$$\frac{1}{q_t} = \frac{1}{K_2 q_e^2} + \frac{t}{q_e} \quad (4)$$

where  $k_2$  is the second-order adsorption rate constant ( $\text{g mol}^{-1} \text{min}^{-1}$ ), slope and intercept were obtained by plotting the data of  $t/q_t$  vs  $t$ . The slope and intercept obtained were  $1/q_e$  and  $1/k_2 q_e^2$ .

The first-order kinetics adsorption of  $\text{Cu}^{2+}$  ion by the liquid-smoke-activated adsorbent was obtained by plotting  $1/t$  and  $t/q_t$ . In contrast, the second-order kinetics was obtained by plotting  $t$  vs  $t/q_t$ . The first- and second-order adsorption kinetics of the liquid-smoke-activated adsorbent are presented in Fig. 9 (a, b).



(a)



(b)

Fig. 9 First- (a) and second-order (b) adsorption kinetics of the liquid-smoke-activated adsorbent

Fig. 9 (a) shows the first-order adsorption kinetics plot for the  $\text{Cu}^{2+}$  ion adsorption system. The kinetic parameters corresponding to the first-order kinetic system of the two kinetic models are given in Table 2. The  $q_e$  values calculated based on first-order kinetic equations were 38.46 and 47.61 mg/g for adsorption at agitation rates of 100 and 200 rpm, respectively. The linear regression coefficient of  $\text{Cu}^{2+}$  ion adsorption by the liquid-smoke-activated adsorbent at 100 rpm was  $R^2=0.994$ , and that at 200 rpm was  $R^2=0.989$ . The

first-order rate constants ( $k_1$ ) at agitation rates of 100 and 200 rpm were evaluated as 387.69 and 490 g/mg min, respectively. The value of  $k_1$  indicates that by using the first-order kinetic model, the process of adsorption taking place on the system is very fast.

The kinetic parameters relating to the second-order kinetic system obtained from the two kinetic models in Fig. 9 (b) are given in Table 2. The  $q_e$  values calculated based on the second-order kinetic equation were 52.63 and 58.82 mg/g at the agitation rates of 100 and 200 rpm, respectively. The correlation coefficient ( $R^2$ ) obtained for the first-order kinetic model was greater than that for the second-order. This implied that the first-order kinetic equation was more appropriate to simulate the kinetic data, and hence that the rate of  $\text{Cu}^{2+}$  adsorption by the activated carbon nanoparticles confirmed to physical adsorption [26].

TABLE II  
THE KINETIC PARAMETERS CORRESPONDING TO THE TWO KINETIC MODELS FOR THE LIQUID-SMOKE-ACTIVATED ADSORBENT

	first-order			second-order		
	$q_e \left(\frac{\text{mg}}{\text{g}}\right)$	$K_1 \left(\frac{\text{g}}{\text{mgmin}}\right)$	$R^2$	$q_e \left(\frac{\text{mg}}{\text{g}}\right)$	$K_2 \left(\frac{\text{g}}{\text{mgmin}}\right)$	$R^2$
100 rpm	38.46	387.69	0.994	52.63	$3.41 \times 10^{-5}$	0.516
200 rpm	47.61	490	0.989	58.82	$2.72 \times 10^{-5}$	0.602

#### IV. CONCLUSION

The highest adsorption efficiency of the activated carbon was 97.5%, obtained after a contact time of 60 min with an initial  $\text{Cu}^{2+}$  concentration of 30 ppm and an agitation speed of 200 rpm. Activated carbon nanoparticles derived from the pyrolysis residue of oil palm shells has proved to be excellent for the adsorption of  $\text{Cu}^{2+}$  at low concentrations (30–60 ppm), but its ability decreases at higher concentrations (> 150 ppm). The kinetic study has shown that the adsorption of  $\text{Cu}^{2+}$  by liquid-smoke-activated carbon nanoparticles is a first-order process that can be fitted by the Freundlich model, with an  $R^2$  coefficient of 0.937.

#### NOMENCLATURE

$C_e$	Concentration of adsorbate in solution	(ppm)
$q_e$	Concentration of bound adsorbate in each gram of adsorbent	(mg/g)
$q_m$	Monolayer adsorption capacity	(mg/g)
$K_l$	Isotherm constant	(L/mg)
$K_f$	Freudlich isotherm constant	(mg/g)
$1/n$	Indicative constant, indicating the intensity of the adsorption process	

#### Abbreviations

FTIR	Fourier-transform infrared spectroscopy
AAS	Atomic Adsorption Spectroscopy
SEM	scanning electron microscopy

#### ACKNOWLEDGMENT

The authors are grateful to the financial support provided by Syiah Kuala University and the Ministry of Research, Technology, and Higher Education of Indonesia.

#### REFERENCES

- [1] J. Dai, W. Wang, W. Wu, J. Gao, and C. Dong, "Adsorption and desorption of  $\text{Cu}^{2+}$  on paddy soil aggregates pretreated with different levels of phosphate," *J. Environ. Sci.*, vol. 55, pp. 311-320, May 2017.
- [2] Y. Zhou, L. Zhang, and Z. Cheng, "Removal of organic pollutants from aqueous solution using agricultural wastes: a review," *J. Mol. Liq.*, vol. 212, pp. 739-762, Dec. 2015.
- [3] Y. Dai, K. Zhang, J. Li, Y. Jiang, Y. Chen, and S. Tanaka, "Adsorption of copper and zinc onto carbon material in an aqueous solution oxidised by ammonium peroxydisulphate," *Sep. Purif. Technol.*, vol. 2, pp. 255-263, Oct. 2017.
- [4] Z.C. Wu, Z.Z. Wang, J. Liu, J.H. Yin, and S.P. Kuang, "A new porous magnetic chitosan modified by melamine for fast and efficient adsorption of Cu (II) ions," *Int J Biol Macromol.*, vol. 81, pp. 838-846, Nov. 2015.
- [5] M.A. Hossain, H.H. Ngo, W.S. Guo, and T.V. Nguyen, "Palm oil fruit shells as biosorbent for copper removal from water and wastewater: experiments and sorption models," *Bioresour. Technol.*, vol. 113, pp. 97-101, Jun 2012.
- [6] E. Gunasundari, and S. Kumar, "Adsorption isotherm, kinetics and thermodynamic analysis of Cu (II) ions onto the dried algal biomass (*Spirulina platensis*)," *J. Ind.Eng. Chem.*, vol. 56, pp. 129-144, Dec. 2017.
- [7] M. Bansal, A. Mudhoo, V.K. Garg, and D. Singh, "Preparation and characterisation of biosorbents and copper sequestration from simulated wastewater," *Int. J. Environ. Sci. Technol.*, vol.11(5), pp. 1399-1412, July 2014.
- [8] Q. Zhu, L. Wang, Z. An, H. Ye, and X. Feng, "Hydrothermal synthesis of silico-manganese nanohybrid for Cu (II) adsorption from aqueous solution," *Appl. Surf. Sci.*, vol. 371, pp. 102-111, May 2016.
- [9] Y. Xue, S. Wu, and M. Zhou, "Adsorption characterisation of Cu (II) from aqueous solution onto basic oxygen furnace slag," *Chem. Eng. J.*, vol. 231, pp. 355-364, Sep. 2013.
- [10] M.O. Ojemaye, O.O. Okoh, and A.I. Okoh, "Adsorption of  $\text{Cu}^{2+}$  from aqueous solution by a novel material; azomethine functionalised magnetic nanoparticles," *Sep. Purif. Technol.*, vol.183, pp.204-215, Aug. 2017.
- [11] L.H. Reddy, J.L. Arias, J. Nicolas, and P. Couvreur, "Magnetic nanoparticles: design and characterisation, toxicity and biocompatibility, pharmaceutical and biomedical applications," *Chem. Rev.*, vol.112(11), pp. 5818-5878, Oct. 2012.
- [12] I. Ali, "New generation adsorbents for water treatment," *Chem. Rev.*, vol. 112(10), pp. 5073-5091, Jun. 2012.
- [13] S.C. Tang, and I.M. Lo, "Magnetic nanoparticles: essential factors for sustainable environmental applications," *Water Res.*, vol. 47(8), pp. 2613-2632, May 2013.
- [14] J. Huang, H. Xie, H. Ye, T. Xie, Y. Lin, Y. J. Gong, C. Jiang, Y. Wu, S. Liu, Y. Cui, and J. Mao, "Effect of carboxyethylation degree on the adsorption capacity of Cu (II) by N-(2-carboxyethyl) chitosan from squid pens," *Carbohydr. Polym.*, vol. 138, pp. 301-308, Mar 2016.
- [15] A. Kamari, S.N.M. Yusoff, F. Abdullah, and W.P. Putra, "Biosorptive removal of Cu (II), Ni (II) and Pb (II) ions from aqueous solutions using coconut dregs residue: adsorption and characterisation studies," *J. Environ. Chem. Eng.*, vol. 2(4), pp. 1912-1919, Dec. 2014.
- [16] Z.N. Garba, I. Bello, A. Galadima, and A.Y. Lawal, "Optimisation of adsorption conditions using central composite design for the removal of copper (II) and lead (II) by defatted papaya seed," *Karbala Int. J Mod. Sci.*, vpl. 2(1), pp. 20-28, Mar 2016.
- [17] H. Koyuncu, and A.R. Kul, "An investigation of Cu (II) adsorption by native and activated bentonite: kinetic, equilibrium and thermodynamic study," *J. Environ. Chem. Eng.*, vol. 2(3), pp. 1722-1730, Sep. 2014.
- [18] W.W. Ngah, L.C. Teong, R.H. Toh, and M.A.K.M. Hanafiah, "Utilisation of chitosan-zeolite composite in the removal of Cu (II) from aqueous solution: adsorption, desorption and fixed bed column studies," *Chem. Eng. J.*, vol. 209, pp. 46-53, Oct. 2012.

- [19] O.H. Kwon, J.O. Kim, D.W. Cho, R. Kumar, S.H. Baek, M.B. Kurade, and B.H. Jeon, "Adsorption of As (III), As (V) and Cu (II) on zirconium oxide immobilised alginate beads in aqueous phase," *Chemosphere*, vol. 160, pp.126-133, Oct. 2016.
- [20] M. Gan, S. Sun, Z. Zheng, H. Tang, J. Sheng, J. Zhu, and X. Liu, "Adsorption of Cr (VI) and Cu (II) by AlPO<sub>4</sub> modified biosynthetic Schwertmannite," *Appl. Surf. Sci.*, vol. 356, pp. 986-997, Nov. 2015.
- [21] Q. Xu, Y. Wang, L. Jin, Y. Wang, and M. Qin, "Adsorption of Cu (II), Pb (II) and Cr (VI) from aqueous solutions using black wattle tannin-immobilised nanocellulose," *J. Hazard Mater.*, vol. 339, pp. 1-99, Oct. 2017.
- [22] M. Faisal, A. Gani, Husni and H. Daimon, "A preliminary study of the utilisation of liquid smoke from palm kernel shells for organic mouthwash," *Int. J. GEOMATE*, vol. 13 (37), pp. 116-120, Sep. 2017.
- [23] M. Faisal, A. Gani, and Abubakar, "Removal of Copper Ions from Aqueous Solution using Palm Shell Charcoal Activated by NaOH," *Int. J. GEOMATE*, vol. 15 (48), pp. 143-147, Aug. 2018.
- [24] M.Faisal, A.Gani, Husni, A.Baihaqi, and H. Daimon, "Pyrolysis of oil palm kernel shell into liquid smoke and its application to control anthracnose disease on chili (capsicum annum L.)," *J. Eng. Appl. Sci.*, vol. 11 (12), pp. 2583-2587, 2016.
- [25] A. Gani, and M. Faisal, "Evaluation of liquid smoke-activated palm kernel shells biochar for cadmium adsorption," *Rasayan J. Chem.*, In press.
- [26] Z. Ma, D. Chen, J. Gu, B. Bao, and Q. Zhang, "Determination of pyrolysis characteristics and kinetics of palm kernel shell using TGA-FTIR and model-free integral methods," *Energy Convers. Manag.*, vol. 89, pp. 251-259, Jan. 2015.
- [27] Z.C. Wu, Z.Z. Wang, J. Liu, J.H. Yin, and S.P. Kuang, "A new porous magnetic chitosan modified by melamine for fast and efficient adsorption of Cu (II) ions," *Int J Biol Macromol.*, vol. 81, pp. 838-846, Nov. 2015.
- [28] Q. He, J. Dai, L. Zhu, K. Xiao, and Y. Yin, "Synthesis and lead absorption properties of sintered activated carbon supported zero-valent iron nanoparticle," *J. Alloys Compd.*, vol. 687, pp. 326-333, Dec. 2016.
- [29] A.S. Semerciöz, F. Göğüş, A. Çelekli, and H. Bozkurt, "Development of carbonaceous material from grapefruit peel with microwave implemented-low temperature hydrothermal carbonisation technique for the adsorption of Cu (II)," *J.Clean. Prod.*, vol. 165, pp. 599-610, Nov. 2017.
- [30] I. Mobasherpour, E. Salahi, and M. Ebrahimi, "Thermodynamics and kinetics of adsorption of Cu (II) from aqueous solutions onto multi-walled carbon nanotubes," *J. Saudi Chem. Soc.*, vol. 18(6), 792-801, Dec. 2014.